Valley spin polarization of Tl/Si(111)

Sebastian D. Stolwijk,[1] Anke B. Schmidt,[1] Kazuyuki Sakamoto,[2] Peter Krüger,[3] and Markus Donath[1,*]

[1]*Physikalisches Institut, Westfälische Wilhelms-Universität Münster, Wilhelm-Klemm-Strasse 10, 48149 Münster, Germany*
[2]*Department of Materials Science, Chiba University, Chiba 263-8522, Japan*
[3]*Institut für Festkörpertheorie, Westfälische Wilhelms-Universität Münster, Wilhelm-Klemm-Strasse 10, 48149 Münster, Germany*

The metal/semiconductor hybrid system Tl/Si(111)-(1×1) exhibits a unique Tl-derived surface state with remarkable properties. It lies within the silicon band gap and forms spin-momentum-locked valleys close to the Fermi energy at the $\bar{K}$ and $\bar{K}'$ points. These valleys are completely spin polarized with opposite spin orientation at $\bar{K}$ and $\bar{K}'$ and show a giant spin splitting of more than 0.5 eV. We present a detailed preparation study of the surface system and demonstrate that the electronic valleys are extremely robust, surviving exposure to 100 L hydrogen and 500 L oxygen. We investigate the influence of additional Tl atoms on the spin-polarized valleys. By combining photoemission and inverse photoemission, we prove the existence of fully spin-polarized valleys crossing the Fermi level. Moreover, these metallic valleys carry opposite Berry curvature at $\bar{K}$ and $\bar{K}'$, very similar to WSe$_2$, promising a large spin Hall effect. Thus, Tl/Si(111)-(1×1) possesses all necessary key properties for spintronic applications.

I. INTRODUCTION

The term *spintronics* is used in information technology and describes the idea of using the spin of the electron in addition to or instead of its charge as an information carrier. Creation, manipulation, and detection of spin polarization are required for the spin to play a functional role in future electronic devices [1–7]. Lifting the spin degeneracy of electronic states, which is a necessary condition for reaching these goals, can be achieved by magnetic exchange interaction or by spin-orbit interaction. While in ferromagnetic solids the magnetization direction is a unique quantization axis for the spin, the situation is much more sophisticated in spin-orbit-influenced systems. Here the preferred spin direction depends not only critically on the wave vector **k** of the electrons but also on the crystal symmetry of the material.

A prerequisite for lifting the spin degeneracy via spin-orbit interaction is a broken inversion symmetry, which appears, in particular, at the surface. Therefore, the current scientific interest is strongly focused on surface systems comprising heavy elements with strong spin-orbit interaction: Rashba systems [8] and topological insulators [9]. In view of applications in electronic devices, promising surface systems for spintronic applications should possess several key properties [10–12]. In particular, one is in the need of a surface state with a large spin-orbit-induced spin splitting, preferably with full spin polarization, and located within a fundamental band gap. Therefore, thin layers of heavy metals on top of semiconducting substrates are of special interest [11–25]. Furthermore, the surface state should be either metallic or, better yet, allow the control of its energetic position relative to the Fermi energy [22]. Finally, if the surface system proves robust against contamination or adsorbates and lives on the technologically relevant Si(111) surface, the system shows promise on the way to integrate spintronic devices on current semiconductor technology.

The honeycomb-layered system Tl/Si(111) could, indeed, constitute such a system. For one monolayer (ML) of Tl on Si(111) [see Fig. 1(a)], a number of occupied and unoccupied spin-orbit split surface states exist in the silicon band gap. The occupied states were intensively studied by spin- and angle-resolved photoemission (ARPES) and show, e.g., a remarkable rotation of the spin direction as a function of the wave vector along the $\bar{\Gamma}\bar{K}$ high-symmetry line [14]. Their spin splitting, however, is largest only far below the Fermi energy.

The unoccupied surface states, in contrast, come close to the Fermi level exactly where they exhibit a giant spin-dependent energy splitting. The unoccupied surface electronic structure of Tl/Si(111) has been investigated with spin- and angle-resolved inverse-photoemission (SRIPE) experiments. An unoccupied surface-derived spin-orbit-split surface state has been identified, which extends throughout the complete surface Brillouin zone and displays a peculiar spin texture—a rotating spin pattern along $\bar{\Gamma}\bar{K}$ [23], a pure in-plane spin polarization along $\bar{\Gamma}\bar{M}$ [26], and a spin texture with a twist around $\bar{M}$ [27].

Special attention has been paid to the valleys at the $\bar{K}$ ($\bar{K}'$) points. SRIPE experiments showed that the valleys are almost completely out-of-plane spin polarized but with opposite orientation at $\bar{K}$ and $\bar{K}'$ [23]. Furthermore, it has been demonstrated that doping of the surface with additional Tl leads to the formation of occupied out-of-plane spin-polarized valleys and, thus, to a unique Fermi surface, where backscattering is strongly suppressed [22].

Hence, of the key properties for spintronic applications, Tl/Si(111) already possesses a surface state with a large spin-orbit-induced spin splitting with full spin polarization located within a fundamental band gap. It can be doped to become metallic and, due to its Si(111) substrate, has the possibility to be integrated into current semiconductor technology.

In this publication we use SRIPE to further determine the potential of the spin-polarized valleys at the $\bar{K}$ ($\bar{K}'$) points for applications in spintronics. To this end, we investigated (i) the robustness of the system and (ii) whether the surface state can be shifted rigidly relative to the Fermi energy. In detail:

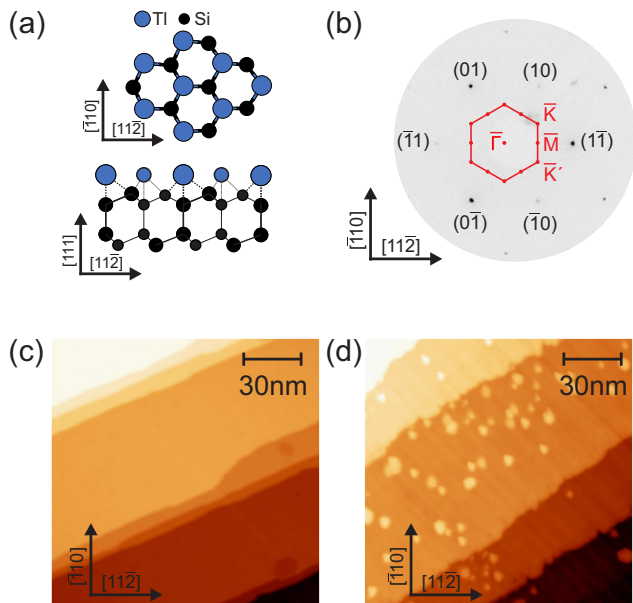*Corresponding author: markus.donath@uni-muenster.de

FIG. 1. (a) Top view and side view of the structural model of the Tl/Si(111)-(1 × 1) surface. (b) LEED image (inverted contrast) of the clean Tl/Si(111)-(1 × 1) surface for a primary electron beam energy $E_p = 85$ eV. The corresponding surface Brillouin zone with the relevant high-symmetry points is indicated in red. (c) STM image of the Tl/Si(111)-(1 × 1) surface (preparation A, 150×150 nm^2, $U = -1$ V, $I = 0.1$ nA). Large terraces with a width of about 50 nm are observed. (d) STM image of the Tl/Si(111)-(1 × 1) surface with about 1.1 ML Tl (preparation A, 140×140 nm^2, $U = 1$ V, $I = 0.1$ nA).

(i) We evaluated the unoccupied surface state around $\bar{K}$ for different surface qualities. It is demonstrated that the homogeneity of the surface strongly influences the surface-state emission. The higher the surface quality the more pronounced is the surface-state emission. Moreover, we conducted adsorbate experiments to demonstrate the robustness of the surface state against contamination, a necessary prerequisite for successful implementation in applications. It is shown that an exposure of 100 L (1 L $= 1.33 \times 10^{-4}$ Pa s) of H$_2$ and 500 L of O$_2$ nearly do not affect the surface state, while exposure to air completely quenches the surface-state emission. For high-quality Tl/Si(111) surfaces, further experiments reveal the valley nature and the complete out-of-plane spin polarization of the unoccupied surface state around $\bar{K}$ ($\bar{K}'$).

(ii) In analogy to the experiment outlined in Ref. [22], we examined the effect of dosage of additional Tl. With ARPES, we confirmed the formation of occupied valleys for Tl coverages of about 1.1 ML. Interestingly, for this coverage, the unoccupied valleys are still observed. This observation is in contradiction to the argumentation of a rigid-shift model in Refs. [21,22].

II. METHODS

The experiments were performed in a multifunction ultrahigh-vacuum (UHV) apparatus with the unique combination of ARPES and SRIPE [28]. Thus, occupied and unoccupied electronic states can be measured in the same

chamber on the same sample preparation. The ARPES data were obtained with a 50 mm simulated hemispherical sector analyzer (SHA50 from Focus GmbH). For excitation, a helium discharge lamp was used providing unpolarized He-I light with an energy of $h\nu = 21.22$ eV. SRIPE experiments were conducted with our homebuilt rotatable spin-polarized electron source [29]. It produces a transversally spin-polarized electron beam with a spin polarization of 29%, whose polarization direction can be chosen freely. This allows measurements of the unoccupied electronic structure with sensitivity to the classical in-plane Rashba spin-polarization direction and, in addition, for non-normal electron incidence, to the out-of-plane spin-polarization direction. Spectra have been normalized to 100% spin polarization of the electron beam [30]. The emitted photons with an energy of $h\nu = 9.9$ eV are detected with a Geiger-Müller-type bandpass detector. The overall energy resolution of the SRIPE experiment is about 350 meV [31]. A detailed description of the SRIPE experiment is given in Refs. [28,32]. Additionally, we employed low-energy electron diffraction (LEED), Auger electron spectroscopy, and scanning tunneling microscopy (STM) for sample characterization. All measurements have been conducted at room temperature.

Our theoretical investigations are based on density-functional theory (DFT) calculations employing a representation of the wave functions by atom-centered Gaussian orbitals together with normconserving pseudopotentials which include spin-orbit coupling. The quasiparticle band structure has been determined within the GW approximation of many-body perturbation theory. For details see Ref. [23].

III. SAMPLE PREPARATION AND CHARACTERIZATION

The adsorption of 1 ML Tl on Si(111) gives rise to a pseudomorphic (1 × 1)-Tl adlayer as shown in Fig. 1(a). Single-monolayer films of Tl on Si(111) were prepared by evaporating Tl from a Ta crucible onto the clean Si(111) substrate at a temperature of 570 K, similar to the recipe given in Ref. [14].

The Si(111) substrates used in this study were cut from a phosphorus-doped Si(111) wafer (n type, 10^{15}/cm^3, 1–5 Ω cm), which had been chemically preoxidized. After insertion into the UHV system, the sample and sample carrier were degassed at about 800 K for several hours, until the base pressure of the UHV chamber ($p \leqslant 1 \times 10^{-10}$ mbar) was restored. Next, the sample was heated to 1230 K for about 1 min by electron bombardment to remove the oxide layer. Subsequently, a flash to 1520 K for about 10 s was applied to remove the carbon contamination from the surface. Temperatures were measured with a pyrometer. A slow cool down is necessary to allow a reordering of the surface atoms. Two cool-down procedures were applied: (A) Cool down to room temperature at a constant rate of 5 K s^{-1}. (B) Moderately fast cooling to 1170 K (10 K s^{-1}), slow cooling ($\leqslant$1 K s^{-1}) through the (1 × 1)-(7 × 7) phase transition at about 1130 K to allow large (7 × 7) reconstructed domains to grow [33], and a more rapid cooling to room temperature. Please note for future reference that Tl-(1 × 1) adlayers grown on Si substrates prepared with procedures A and B are referred to as preparations A and B, respectively.
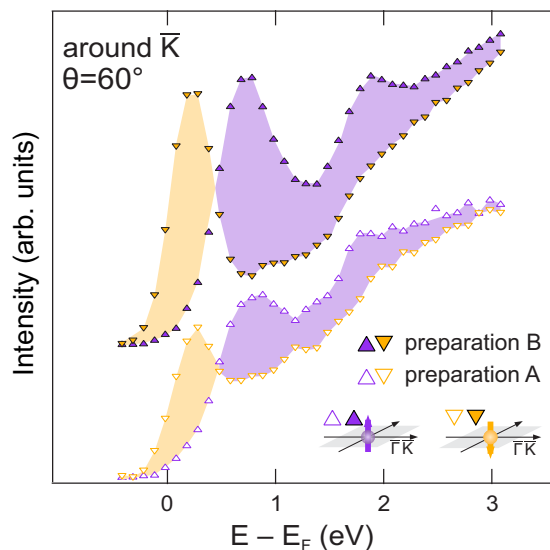
FIG. 2. SRIPE spectra of Tl/Si(111)-(1 × 1) around $\bar{K}$ obtained for preparation A (open purple up-pointing and orange down-pointing triangles) and B (filled purple up-pointing and orange down-pointing triangles). The spectra were measured at an incidence angle of $\theta = 60°$ with sensitivity to the out-of-plane spin-polarization direction.

Both cool-down procedures lead to clean Si(111)-(7 × 7) surfaces with high crystalline quality. However, in comparison with procedure A, procedure B led to even more homogeneous surfaces. We conclude this from the substantially enhanced surface-state intensities of the adlayer system in SRIPE. Surface states are known to be sensitive indicators of the surface quality: The lower the surface roughness, the more homogeneous the surface, and the higher the crystallographic order, the higher is the spectral intensity of the surface-state emission. Figure 2 shows a comparison of SRIPE data for the two different preparation methods A and B. Obviously the films prepared with method B (upper spectra) exhibit more pronounced surface-state emissions, evident in the much larger intensities of the two lowest-lying peaks. It seems that the homogeneity of the Si substrate directly influences the homogeneity of the Tl/Si(111)-(1 × 1) films. Note that the surface quality only affects the spectral intensities. The $E(\mathbf{k}_{\parallel})$ dispersion is almost identical [32], as shown in Fig. 3(a). Frequent flashing led to a degradation of the crystalline quality. Therefore, the substrate was replaced after a couple of preparations.

During evaporation of Tl, the pressure was below 1×10^{-10} mbar. At a substrate temperature of 570 K, the formation of a 1 ML thick film is a self-terminating process. The sharp diffraction pattern and low background intensity observed in the LEED image in Fig. 1(b) reflect a well-ordered (1 × 1) structure. No traces of contaminants are detected with Auger-electron spectroscopy (not shown). Scanning tunneling images of the Tl/Si(111)-(1 × 1) sample indicate large terraces (≈50 nm) imposed by the Si substrate. Other preparation methods as, e.g., presented in Ref. [18], were tested and led to similar film qualities.
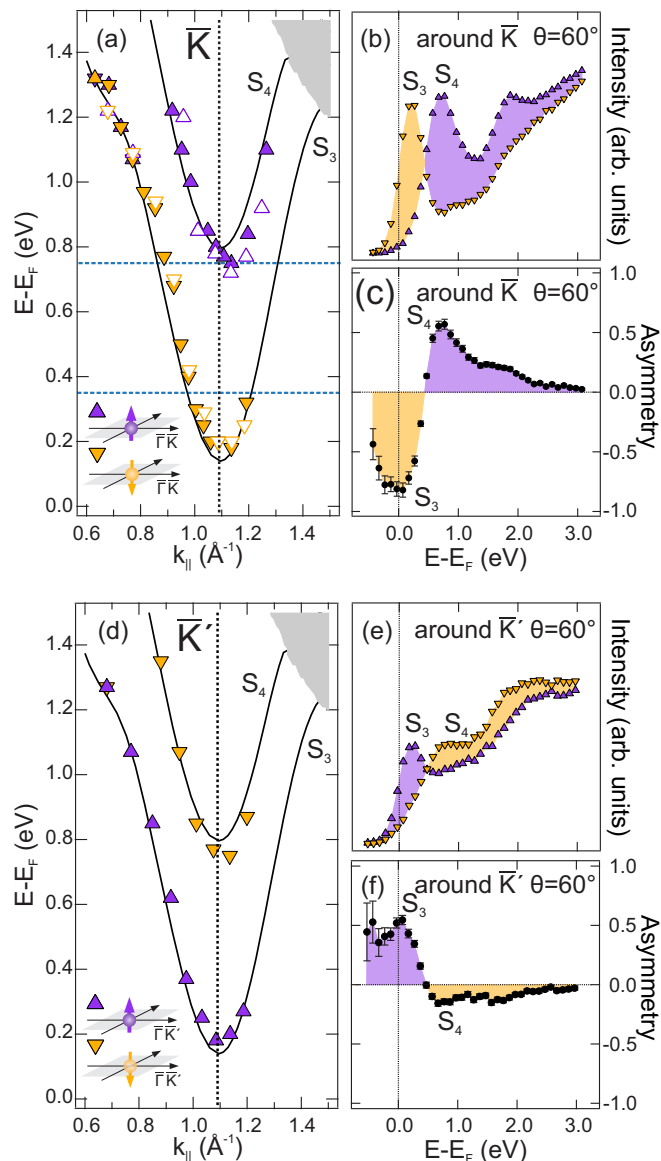

FIG. 3. Surface electronic structure of Tl/Si(111)-(1 × 1) around $\bar{K}$ (a) and $\bar{K}'$ (d). Filled and open triangles were obtained for preparations A and B, respectively. Solid lines represent the calculated surface-state bands and gray-shaded areas denote the projected bulk bands [23]. Blue dashed lines indicate where the constant-energy maps shown in Fig. 4 were measured. (b) and (e) SRIPE spectra (preparation B) with sensitivity to the out-of-plane spin polarization around $\bar{K}$ and $\bar{K}'$, respectively, with corresponding out-of-plane spin asymmetry shown in (c) and (f).

Tl/Si(111)-(1 × 1) films with a small extra amount of Tl, e.g., 1.1 ML films, were grown by evaporating about two monolayers of Tl onto the Si substrate kept at room temperature. Subsequently, the sample was annealed to 500 K, while monitoring the LEED pattern. With advancing annealing time, the formation of a (1 × 1) structure was observed. Stopping the annealing, before a sharp unchanging LEED pattern was observed, led to Tl/Si(111)-(1 × 1) films with a small extra amount of Tl. The STM image in Fig. 1(d) shows a Tl/Si(111)-(1 × 1) film with a coverage of about 1.1 ML.
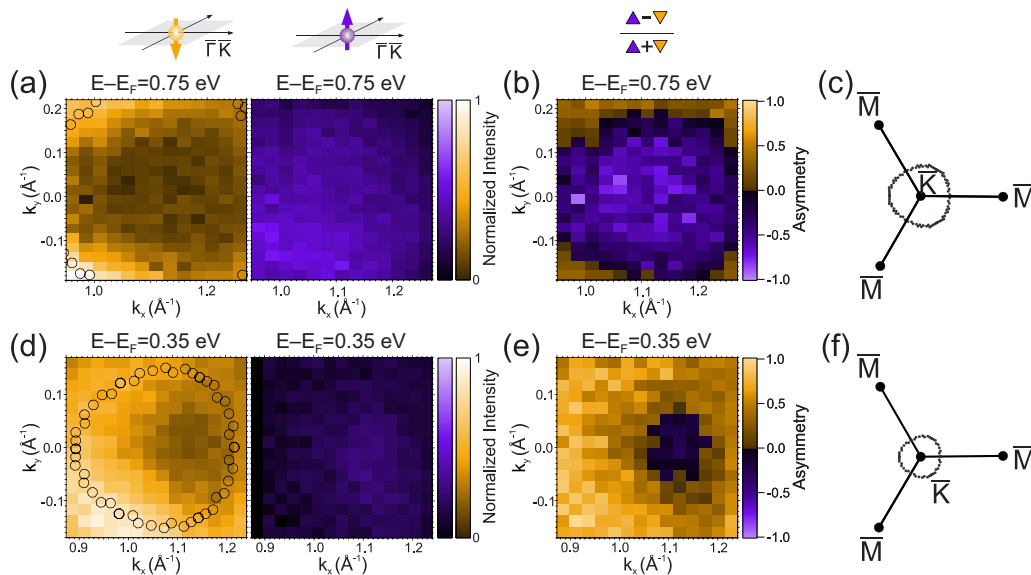
FIG. 4. Constant-energy maps for the two out-of-plane spin directions of Tl/Si(111)-(1 × 1) (preparation B) around $\bar{K}$ at (a) $E - E_F = 0.75$ eV and (d) $E - E_F = 0.35$ eV. The open circles show the calculated contour of the lower lying surface-state component S_3 [see (c) and (f)]. (b) and (e) The corresponding spin-asymmetry data. Calculated constant-energy maps at (c) $E - E_F = 0.75$ eV and (f) $E - E_F = 0.35$ eV.

IV. COMPLETELY SPIN-POLARIZED VALLEYS

Figure 3 presents spin-revolved IPE results of Tl/Si(111) surfaces in the vicinity of $\bar{K}$ and $\bar{K}'$. At these high-symmetry points, the surface-state components S_3 and S_4 approach the Fermi energy E_F and form spin-split valleys. Notably, at the $\bar{K}$ and $\bar{K}'$ points, the same features appear with opposite spin asymmetry [compare spectra in Figs. 3(b) and 3(e)]. The spin-asymmetry data in Figs. 3(c) and 3(f) around $\bar{K}$ and $\bar{K}'$, respectively, underline this reversal. Spin-asymmetry values of more than 80% around $\bar{K}$ and 60% around $\bar{K}'$ are found (without background subtraction).

In Figs. 4(a) and 4(d) the dispersion around $\bar{K}$ is further analyzed by spin-resolved constant-energy maps at $E = 0.75$ eV and $E = 0.35$ eV, respectively [see dashed lines in Fig. 3(a)]. For each point of the constant-energy plots, the electron incidence angle θ and the azimuthal angle φ of the sample are set in such a way that the SRIPE measurement is carried out at a distinct value for k_x and k_y. The intensity for each spin direction (out-of-plane) is represented by the brightness of the corresponding color. Thus, Figs. 4(a) and 4(d) represent spin-resolved momentum distribution maps of the surface state. The corresponding spin-asymmetry maps are presented in Figs. 4(b) and 4(e).

At $E = 0.75$ eV, the constant-energy scan crosses the surface-state component S_3 and grazes the bottom of S_4. At $E = 0.35$ eV, only the lower lying surface-state component S_3 is measured. The results reveal S_3 as a ringlike feature, which is in good agreement with theoretical calculations [see Fig. 4(f)]. The trigonal warping is found to be a consequence of the threefold symmetry. A trigonal warping is also predicted for MoS_2 [34], a system with similar out-of-plane spin-polarized valleys. The bottom of S_4 is detected as a circular feature. The spin-asymmetry data provide proof of the out-of-plane but opposite spin polarization of S_3 and S_4. Evidently, around $\bar{K}$ and $\bar{K}'$, S_3 and S_4 form out-of-plane spin-polarized valleys with almost parabolic shape.

Figure 5 shows a measurement of the out-of-plane spin-resolved spectral intensity at an energy of 0.2 eV as a function of the azimuth φ of the sample. With k_x and k_y being the components of $\mathbf{k}_\parallel$ in the x and y direction, respectively [see illustration in Fig. 5(a)], the measurement represents a momentum distribution curve with constant $k_\parallel = \sqrt{k_x^2 + k_y^2}$ but varying k_x and k_y components (blue dashed line). At $\bar{K}$ and $\bar{K}'$, the measurement crosses the lower lying unoccupied surface-state component S_3. Clearly S_3 is out-of-plane spin polarized antiparallel to the surface normal at $\bar{K}$ and out-of-plane spin polarized parallel to the surface normal at $\bar{K}'$. The different spectral intensities at $\bar{K}$ and $\bar{K}'$ are attributed to the threefold symmetry of the surface in combination with the experimental geometry. Furthermore, the data show that the background intensity is unpolarized.
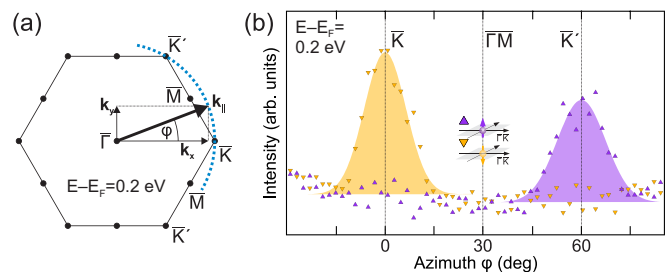

FIG. 5. (a) Illustration and (b) results of a constant-$k_\parallel$ ($k_\parallel \approx 1.1$Å) measurement of Tl/Si(111)-(1 × 1) (preparation B) at a constant energy of $E - E_F = 0.2$ eV for $\theta = 60°$. $k_\parallel = \sqrt{k_x^2 + k_y^2}$ is fixed, while k_x and k_y are varied by changing the sample azimuthal angle $\varphi = \arctan\frac{k_y}{k_x}$. The measurement crosses the lower-lying surface-state component S_3 at $\bar{K}$ and $\bar{K}'$. The experiment is sensitive to the out-of-plane spin-polarization direction (purple up-pointing and orange down-pointing triangles).
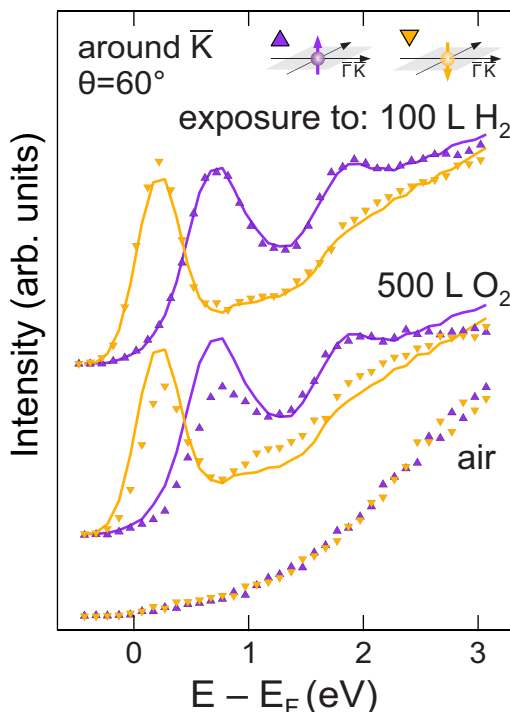
FIG. 6. SRIPE spectra around $\bar{K}$ on preparation B for a surface exposed to 100 L of H_2, 500 L of O_2, and air at ambient pressure (filled purple up-pointing and orange down-pointing triangles). Spectra for the clean surface are shown as solid lines (same data as in Fig. 2, preparation B).

We have thus established that the Tl/Si(111)-(1 × 1) surface carries an unoccupied spin-split surface state within the silicon band gap that approaches the Fermi energy at the $\bar{K}$ and $\bar{K}'$ points, where it forms parabolic valleys. Our results show that these valleys are completely out-of-plane spin polarized in the vicinity of E_F with opposite sign at $\bar{K}$ and $\bar{K}'$ and the next state with opposite spin polarization about 0.5 eV higher in energy.

V. ROBUSTNESS AGAINST CONTAMINATION

With the goal in mind to integrate the Tl/Si(111)-(1 × 1) surface system into a possible device, it has to demonstrate some robustness against contamination or adsorbates. A standard approach to identify surface states is to expose the surface to gas contaminants and, thereby, intentionally increase the amount of surface impurities. Typically, an exposure to a few L of, e.g., oxygen (O_2) or hydrogen (H_2), already suffices to completely quench surface-state emissions (see for example Refs. [35,36]). Figure 6 shows SRIPE measurements sensitive to the out-of-plane spin-polarization direction around $\bar{K}$, which are obtained after an exposure to 100 L H_2, to 500 L O_2, and to air. The starting point of each adsorbate experiment is the clean Tl/Si(111)-(1 × 1) surface (preparation B, shown as solid lines).

Although the surface-state emissions are quenched after exposure to air, exposure to 100 L H_2 and 500 L O_2 has almost no effect on the observed spectral intensities of S_3
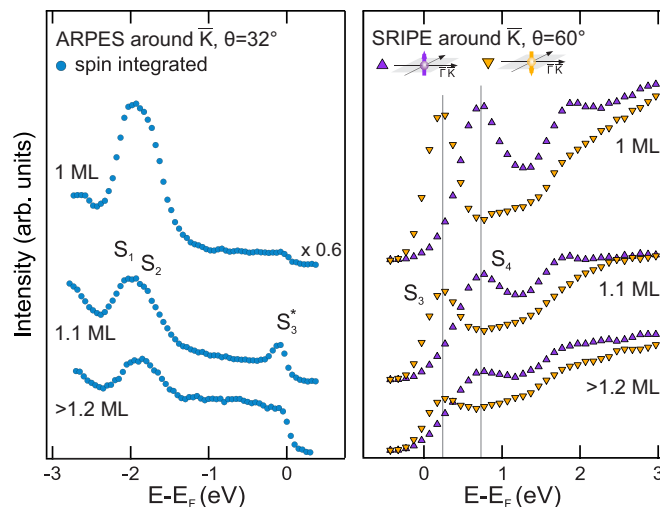

FIG. 7. Left: ARPES measurements ($\hbar\omega = 21.22$ eV) around $\bar{K}$ of 1 ML Tl/Si(111)-(1 × 1) (preparation B) and Tl/Si(111)-(1 × 1) surfaces with more than 1 ML Tl. Right: Corresponding SRIPE measurements with sensitivity to the out-of-plane spin-polarization direction.

and S_4. This inert behavior is very atypical for surface-state emissions. However, in the case of Tl/Si(111)-(1 × 1), the robust behavior of the surface states to foreign adsorbates reflects the electronically saturated nature of the surface dangling bonds [37]. The dangling bonds of the Si atoms are saturated by the electrons from the Tl adatoms and the surface becomes extremely inert. This is also the reason for the self-termination at a coverage of one monolayer of Tl (cf. Sec. III).

VI. TOWARDS METALLIC VALLEYS

The unoccupied surface state found on the pristine Tl/Si(111)-(1 × 1) surface gives rise to almost completely out-of-plane spin-polarized valleys close to the Fermi level at the $\bar{K}$ and $\bar{K}'$ points. However, spintronic applications rely on metallic spin-polarized states. In the following, it will be demonstrated that the valleys become metallic by adding more Tl to the Tl/Si(111)-(1 × 1) surface. In this light, the unique properties of the Tl/Si(111)-(1 × 1) surface may open up an avenue to improve the efficiency of spin currents for silicon spintronics applications [22].

Previous spin-resolved ARPES measurements detected occupied out-of-plane spin-polarized valleys for Tl/Si(111)-(1 × 1) surfaces with Tl coverages of more than 1 ML [22]. It is argued that the metallic valleys result from a down shift of the unoccupied surface-state component S_3 due to electron doping by the additional Tl atoms. Metallic valleys are also found for the isoelectronic Tl/Ge(111)-(1 × 1) surface [21]. Here it is assumed that the occupation of adsorption sites at surface defects by a small excess of Tl atoms leads to electron doping mainly for the states localized in the topmost Tl layer.

ARPES and SRIPE measurements on surfaces with additional Tl are presented in Fig. 7. Surfaces with Tl coverages exceeding 1 ML were prepared as described in Sec. III. The Tl

coverage was determined by STM and by a comparison of the ARPES data obtained in this experiment with the spin-resolved ARPES data presented in Ref. [22]. Tl coverages of (i) 1 ML, (ii) approximately 1.1 ML (see STM image in Fig. 2), and (iii) above 1.2 ML are analyzed. The SRIPE and ARPES spectra were taken around the $\bar{K}$ point. It is important to note that, for each coverage, the same sample preparation was measured with SRIPE and ARPES in the same apparatus.

(i) For 1 ML, the SRIPE spectra show the unoccupied surface-state components S_3 and S_4. The ARPES spectrum reveals the (nonresolved) occupied surface-state emissions S_1 and S_2. To separate the two states, spin resolution, sensitive to the out-of-plane spin-polarization direction of the emitted electrons is necessary [22]. The SRIPE spectra show the unoccupied surface-state components S_3 and S_4. Close to E_F, no occupied spectral feature is detected. A Fermi level cutoff is observed, which indicates a metalliclike character of the Tl/Si(111)-(1 × 1) surface. STM studies on Tl/Si(111)-(1 × 1) show that this may be a result of surface defects, which lead to an increased density of states near the Fermi level [18].

(ii) At a coverage of about 1.1 ML, the spectral intensities of S_1 and S_2 decrease and an occupied state S_3^* appears at about 70 meV below the Fermi level. The data agree with spin-resolved ARPES data for a coverage of 1.12 ML from Ref. [22]. S_3^* was interpreted as the former unoccupied surface state S_3, shifted to lower energy [22]. However, no energy shift is observed for S_3 and S_4 in the corresponding SRIPE data. Here only a decrease of the spectral intensities with increased linewidths is observed.

(iii) For coverages above 1.2 ML, S_3^* can no longer be identified. However, the ARPES measurements show increased structureless intensity between E_F and S_1/S_2. This is accompanied by a further decrease of the spectral intensities of S_1, S_2, S_3, and S_4. Again, no shift of S_3 and S_4 is detected.

The decrease of all spectral intensities S_1 to S_4 with accompanying increase in linewidths for coverages above 1 ML indicates a reduction of the surface quality. The higher the excess amount of Tl atoms, the higher is the surface roughness and the lower the spectral intensities of the surface-state emissions. However, no indication of a peak shift for S_3 and S_4 with increasing Tl coverage can be found in our SRIPE spectra. We have emphasized this by adding vertical lines at the energetic positions of S_3 and S_4 in Fig. 7.

Although we observe no shift in energy of the surface states with increasing Tl coverage, we have demonstrated the simultaneous existence of S_3 and S_3^* on the same sample. Line broadening and increased structureless intensities in the ARPES and IPE spectra complicate the interpretation of our results. Consequently, we cannot exclude that the appearance of S_3^* is caused by line broadening effects due to roughening of the surface. Based on our observations, i.e., no shift of S_3 and S_4 in combination with a simultaneous appearance of S_3 and S_3^*, we favor the assumption that the Tl/Si(111)-(1 × 1) structure coexists with patches with additional Tl, where electron doping is effective.

Independent of the interpretation of S_3^*, Tl/Si(111)-(1 × 1) surfaces with a Tl coverage of about 1.1 ML give rise to
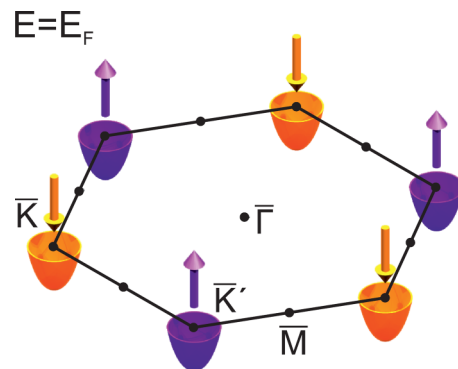

FIG. 8. Visualization of the Fermi surface of the doped Tl/Si(111)-(1 × 1) surface. Completely out-of-plane but oppositely spin-polarized valleys are formed at $\bar{K}$ and $\bar{K}'$ (after Ref. [22]).

metallic, completely out-of-plane spin-polarized valleys at the $\bar{K}$ ($\bar{K}'$) points. The spin polarization is opposite at $\bar{K}$ and $\bar{K}'$ and no other states cross the Fermi level. This leads to a Fermi surface as illustrated in Fig. 8. Thus, spin transport is solely determined by the valleys.

Moreover, Tl/Si(111) is a very promising system in the context of valleytronics and spintronics. The topology of its band structure allows for an intrinsic spin Hall effect where electrons with antipodal spin flow to opposite sides of the sample when an electrical field is applied in the surface plane. This is indicated by the opposite Berry curvature at the $\bar{K}$ and $\bar{K}'$ valleys. The curvature values at $\bar{K}$, as resulting from our calculations [38,39], are −29.7 and −66.8 bohr^2 for S_3 and S_4, respectively. These values are of the same size as for monolayers of group-VI dichalcogenides, such as WSe$_2$, that have recently attracted strong interest in this field [40–43]. Consequently, comparably large charge-to-spin conversion effects are to be expected in the electron doped Tl/Si(111) system.

VII. CONCLUSION

In the metal/semiconductor hybrid system Tl/Si(111)-(1 × 1), a unique Tl-derived surface state exists with remarkable properties. It lies within the silicon band gap, is fully unoccupied, but approaches the Fermi level at the $\bar{K}$ and $\bar{K}'$ points. At these points, it also exhibits a giant spin splitting of more than 0.5 eV and forms fully out-of-plane spin-polarized valleys with opposite spin orientation at the $\bar{K}$ and $\bar{K}'$ points. We presented a detailed preparation study for the Tl/Si(111) system and demonstrated that the surface state survives exposure to 100 L hydrogen and 500 L oxygen, thus proving the state extremely robust. Additional Tl on the surface system leads to metallic valleys that form a remarkable Fermi surface, indicating interesting spin-dependent transport properties. Moreover, these valleys carry opposite Berry curvature at $\bar{K}$ and $\bar{K}'$, very similar to WSe$_2$, promising a large spin Hall effect. We have thus established that Tl/Si(111)-(1 × 1) possesses all necessary key properties for spintronic applications.

[1] S. Datta and B. Das, Appl. Phys. Lett. **56**, 665 (1990).

[2] D. Hägele, M. Oestreich, W. W. Rühle, N. Nestle, and K. Eberl, Appl. Phys. Lett. **73**, 1580 (1998).

[3] J. M. Kikkawa and D. D. Awschalom, Nature (London) **397**, 139 (1999).

[4] S. A. Wolf, D. D. Awschalom, R. A. Buhrman, J. M. Daughton, S. von Molnár, M. L. Roukes, A. Y. Chtchelkanova, and D. M. Treger, Science **294**, 1488 (2001).

[5] I. Žutić, J. Fabian, and S. Das Sarma, Rev. Mod. Phys. **76**, 323 (2004).

[6] D. D. Awschalom and M. E. Flatte, Nat. Phys. **3**, 153 (2007).

[7] S. Nadj-Perge, S. M. Frolov, E. P. A. M. Bakkers, and L. P. Kouwenhoven, Nature (London) **468**, 1084 (2010).

[8] Y. A. Bychkov and E. I. Rashba, JETP Lett. **39**, 78 (1984).

[9] M. Z. Hasan and C. L. Kane, Rev. Mod. Phys. **82**, 3045 (2010).

[10] J. Sinova, D. Culcer, Q. Niu, N. A. Sinitsyn, T. Jungwirth, and A. H. MacDonald, Phys. Rev. Lett. **92**, 126603 (2004).

[11] I. Gierz, T. Suzuki, E. Frantzeskakis, S. Pons, S. Ostanin, A. Ernst, J. Henk, M. Grioni, K. Kern, and C. R. Ast, Phys. Rev. Lett. **103**, 046803 (2009).

[12] K. Yaji, Y. Ohtsubo, S. Hatta, H. Okuyama, K. Miyamoto, T. Okuda, A. Kimura, H. Namatame, M. Taniguchi, and T. Aruga, Nat. Commun. **1**, 17 (2010).

[13] I. Barke, F. Zheng, T. K. Rügheimer, and F. J. Himpsel, Phys. Rev. Lett. **97**, 226405 (2006).

[14] K. Sakamoto, T. Oda, A. Kimura, K. Miyamoto, M. Tsujikawa, A. Imai, N. Ueno, H. Namatame, M. Taniguchi, P. E. J. Eriksson, and R. I. G. Uhrberg, Phys. Rev. Lett. **102**, 096805 (2009).

[15] S. Hatta, T. Aruga, Y. Ohtsubo, and H. Okuyama, Phys. Rev. B **80**, 113309 (2009).

[16] S. Mathias, A. Ruffing, F. Deicke, M. Wiesenmayer, I. Sakar, G. Bihlmayer, E. V. Chulkov, Y. M. Koroteev, P. M. Echenique, M. Bauer, and M. Aeschlimann, Phys. Rev. Lett. **104**, 066802 (2010).

[17] T. Okuda, K. Miyamoto, Y. Takeichi, H. Miyahara, M. Ogawa, A. Harasawa, A. Kimura, I. Matsuda, A. Kakizaki, T. Shishidou, and T. Oguchi, Phys. Rev. B **82**, 161410(R) (2010).

[18] P. Kocán, P. Sobotík, and I. Ošt'ádal, Phys. Rev. B **84**, 233304 (2011).

[19] A. Takayama, T. Sato, S. Souma, and T. Takahashi, Phys. Rev. Lett. **106**, 166401 (2011).

[20] P. Höpfner, J. Schäfer, A. Fleszar, J. H. Dil, B. Slomski, F. Meier, C. Loho, C. Blumenstein, L. Patthey, W. Hanke, and R. Claessen, Phys. Rev. Lett. **108**, 186801 (2012).

[21] Y. Ohtsubo, S. Hatta, H. Okuyama, and T. Aruga, J. Phys.: Condens. Matter **24**, 092001 (2012).

[22] K. Sakamoto, T.-H. Kim, T. Kuzumaki, B. Müller, Y. Yamamoto, M. Minoru Ohtaka, J. Osiecki, K. Miyamoto, Y. Takeichi, A.

Harasawa, S. D. Stolwijk, A. B. Schmidt, J. Fujii, R. I. G. Uhrberg, M. Donath, H. W. Yeom, and T. Oda, Nat. Commun. **4**, 2073 (2013).

[23] S. D. Stolwijk, A. B. Schmidt, M. Donath, K. Sakamoto, and P. Krüger, Phys. Rev. Lett. **111**, 176402 (2013).

[24] L. V. Bondarenko, D. V. Gruznev, A. A. Yakovlev, A. Y. Tupchaya, D. Usachov, O. Vilkov, A. Fedorov, D. V. Vyalikh, S. V. Eremeev, E. V. Chulkov, A. V. Zotov, and A. A. Saranin, Sci. Rep. **3**, 1826 (2013).

[25] P. Eickholt, P. Krüger, S. D. Stolwijk, A. B. Schmidt, and M. Donath, Phys. Rev. B **93**, 085412 (2016).

[26] S. D. Stolwijk, K. Sakamoto, A. B. Schmidt, P. Krüger, and M. Donath, Phys. Rev. B **90**, 161109(R) (2014).

[27] S. D. Stolwijk, K. Sakamoto, A. B. Schmidt, P. Krüger, and M. Donath, Phys. Rev. B **91**, 245420 (2015).

[28] M. Budke, T. Allmers, M. Donath, and G. Rangelov, Rev. Sci. Instrum. **78**, 113909 (2007).

[29] S. D. Stolwijk, H. Wortelen, A. B. Schmidt, and M. Donath, Rev. Sci. Instrum. **85**, 013306 (2014).

[30] M. Donath, Appl. Phys. A **49**, 351 (1989).

[31] M. Budke, V. Renken, H. Liebl, G. Rangelov, and M. Donath, Rev. Sci. Instrum. **78**, 083903 (2007).

[32] S. D. Stolwijk, *Spin-Orbit-Induced Spin Textures of Unoccupied Surface States on Tl/Si(111)* (Springer, New York, 2015).

[33] U. Höfer, L. Li, G. A. Ratzlaff, and T. F. Heinz, Phys. Rev. B **52**, 5264 (1995).

[34] A. Kormányos, V. Zólyomi, N. D. Drummond, P. Rakyta, G. Burkard, and V. I. Fal'ko, Phys. Rev. B **88**, 045416 (2013).

[35] W. Altmann, M. Donath, V. Dose, and A. Goldmann, Solid State Commun. **53**, 209 (1985).

[36] B. Reihl, R. R. Schlittler, and H. Neff, Phys. Rev. Lett. **52**, 1826 (1984).

[37] S. S. Lee, H. J. Song, K. D. Kim, J. W. Chung, K. Kong, D. Ahn, H. Yi, B. D. Yu, and H. Tochihara, Phys. Rev. B **66**, 233312 (2002).

[38] We have adapted the algorithm presented in Ref. [39] for the computation of the Berry curvature on the DFT level.

[39] J. Kübler and C. Felser, Phys. Rev. B **85**, 012405 (2012).

[40] D. Xiao, G.-B. Liu, W. Feng, X. Xu, and W. Yao, Phys. Rev. Lett. **108**, 196802 (2012).

[41] K. F. Mak, K. He, J. Shan, and T. F. Heinz, Nat. Nano. **7**, 494 (2012).

[42] H. Zeng, J. Dai, W. Yao, D. Xiao, and X. Cui, Nat. Nano. **7**, 490 (2012).

[43] W. Feng, Y. Yao, W. Zhu, J. Zhou, W. Yao, and D. Xiao, Phys. Rev. B **86**, 165108 (2012).